ADVANCED ENGINEERING MATERIALS
www.aem-journal.com

The Effect of Equal Channel Angular Pressing on Coarsening Kinetics of AZ80–0.2Y–0.15Ca Alloy in Semisolid State

*Lingling Fan, Mingyang Zhou, Lingbao Ren, Houyi Li, Hongtao Zhang, Tianhui Lu, Chongliang Liu, and Gaofeng Quan**

Semisolid samples of the AZ80–0.2Y–0.15Ca wt% (AZ80M) magnesium alloy are fabricated using equal channel angular pressing (ECAP) followed by semisolid isothermal heating treatment. The effect of the number of ECAP passes on the coarsening dynamics of the alloy at different semisolid temperatures is investigated. The results show that as the number of ECAP passes increases, the coarsening rate constant (*K*) shows a similar trend downward and then upward at different temperatures. And the *K* value of the sample after three passes of ECAP processing (3P) is the lowest, which is primarily attributed to the maximum proportion of high-angle grain boundaries (HAGBs) and the most uniform grain size in the 3P sample. At high solid fractions, a high proportion of HAGBs hinders the coalescence of the adjacent solid grains. At low solid fractions, uniform and fine grains result in insufficient driving force for the Ostwald ripening process. These lead to the lowest *K* value in the 3P sample.

1. Introduction

Magnesium (Mg) alloys, as viable candidates for lightweight construction, are widely used in various fields, including the aerospace, rail transportation, and automotive fields, because of their low densities and high specific strengths.[1,2] However, Mg alloys often show extremely low workability at room temperature because of the hexagonal close packed crystal structure of the alloy and limited independent slip systems of this structure.[3] Therefore, magnesium alloys can only be formed by warm or hot working. These conventional hot working processes are inefficient, which restricts their commercial applications.[4] The semisolid forming method can overcome the shortcomings of the low forming efficiency of magnesium alloy and realize mass production. Strain-induced melt activation (SIMA), hot working above the recrystallization temperature with subsequent reheating to the semisolid state, is the most promising method for preparing semisolid billets because of the high production efficiency and low equipment cost of the manufacturing process.[5] The conventional hot-deformation methods such as hot extrusion, rolling, and forging decrease the size of the initial ingots. The strain introduced into the blank is limited and inhomogeneous. It is not conducive to the formation of uniform and fine solid grains during the subsequent partial remelting process. Equal channel angular pressing (ECAP) is a promising deformation method, which has the advantage of producing metal billets containing a large and strain without the variations of shape and dimension.[6]

The size and roundness of solid grains are two critical factors for the thixoforming of semisolid billets. Solid grains with low roundness are not conducive to the smooth progress of thixoforming, and coarse solid grains will worsen the mechanical properties of thixotropic parts.[7] Therefore, it is necessary to minimize the size of solid particles and maximize their roundness to obtain excellent thixotropic products. As a matter of fact, the coarsening and spheroidizing processes are controlled by the coarsening dynamics of solid grains during partial remelting. The smaller the coarsening dynamics is, the more favorable for the alloy to maintain fine solid grains after thixoforming. Although a considerable amount of work has been devoted to the preparation of semisolid billets using the SIMA method, the studies have mainly focused on the effect of processing parameters on the semisolid microstructure, including liquid fraction and the size and roundness of solid grains.[8–10] Conversely, there is scanty research on the processing parameters

L. Fan, H. Zhang, T. Lu, C. Liu, Prof. G. Quan
Key Laboratory of Advanced Technologies of Materials
Ministry of Education
School of Material Science and Engineering
Southwest Jiaotong University
Chengdu, Sichuan 610031, China
E-mail: quangf@swjtu.cn

Dr. M. Zhou
Science and Technology on Reactor System Design Technology Laboratory
Nuclear Power Institute of China
Chengdu 610213, China

Dr. L. Ren
State Key Laboratory for Mechanical Behavior of Materials
Center for Advancing Materials Performance from the Nanoscale
Xi'an Jiaotong University
Xi'an 710049, China

H. Li
AVIC Jonhon Optronic Technology Co., Ltd.
Luoyang, Henan 471000, China

The ORCID identification number(s) for the author(s) of this article can be found under https://doi.org/10.1002/adem.202000415.

DOI: 10.1002/adem.202000415

of coarsening dynamics of solid grains. Binesh and Aghaie-Khafri[11] studied the effect of repetitive upsetting-extrusion (RUE) processing cycles on the coarsening rate constant (K) of 7075Al alloy at 600 °C. The result suggested that the K value gradually rose with the number of RUE cycles increasing from one to four, which could be attributed to superior atomic diffusion caused by a larger amount of liquid fraction. Fu et al.[12] researched the effect of the number of ECAP passes on the K value of 7075Al alloy at 600 °C, and a similar result was obtained that raising the number of ECAP passes from one to four led to the increase of the K value. Binesh et al.[13] studied the variation of the K values of 7075Al alloy specimens with compression strains of 10%, 20%, 40%, and 55% following isothermal holding temperatures of 600, 610, and 620 °C. The results showed that at 600 and 610 °C, the K value gradually increased with increasing compression strains. However, when the isothermal holding temperature was raised to 620 °C, increasing compression strain from 10% to 40% led to an increase in the K value; increasing compression strain to 50% brought about a decrease in K value. However, the author did not clearly explain the reason for the variation of the K values caused by the increase of strain at different temperatures. Thus, a clear connection between predeformation processing and the coarsening dynamics has not yet been established in the semisolid system. In addition, previous studies on the coarsening dynamics have generally focused on aluminum (Al) alloys. Therefore, more investigations are needed to re-examine Mg alloys, which will provide precious guidance for applying of the semi-solid processing technology to Mg alloys.

In this study, semisolid samples of the AZ80–0.2Y–0.15Ca wt% (AZ80M) magnesium alloy were fabricated using ECAP followed by semisolid isothermal heating treatment. The effect of the number of ECAP passes on the coarsening dynamics of the AZ80M alloy at different semisolid heating temperatures was systematically investigated. The factors affecting the coarsening dynamics of the semisolid alloys were analyzed by referring to the microstructures of the deformed and semisolid samples. In addition, the K values of the semisolid Mg alloys produced using different routes were compared and analyzed in detail.

2. Results and Discussion

2.1. Microstructures of As-Received and ECAP-Processed AZ80M Alloys

Figure 1 shows the electron back-scattered diffraction (EBSD) inverse pole figures (IPFs) and corresponding grain size distributions of as-received and ECAP-processed AZ80M alloy. After one pass of ECAP processing, the grain size of the AZ80M alloy was refined marginally. However, increasing the number of passes from two to three resulted in an apparent refinement of the grain size. The grain size distribution of the 3P alloy was narrowest. This means that the grain size of the 3P sample was the most uniform in all deformed samples. Moreover, it ranged from 1.07 to 11.71 μm and its average value

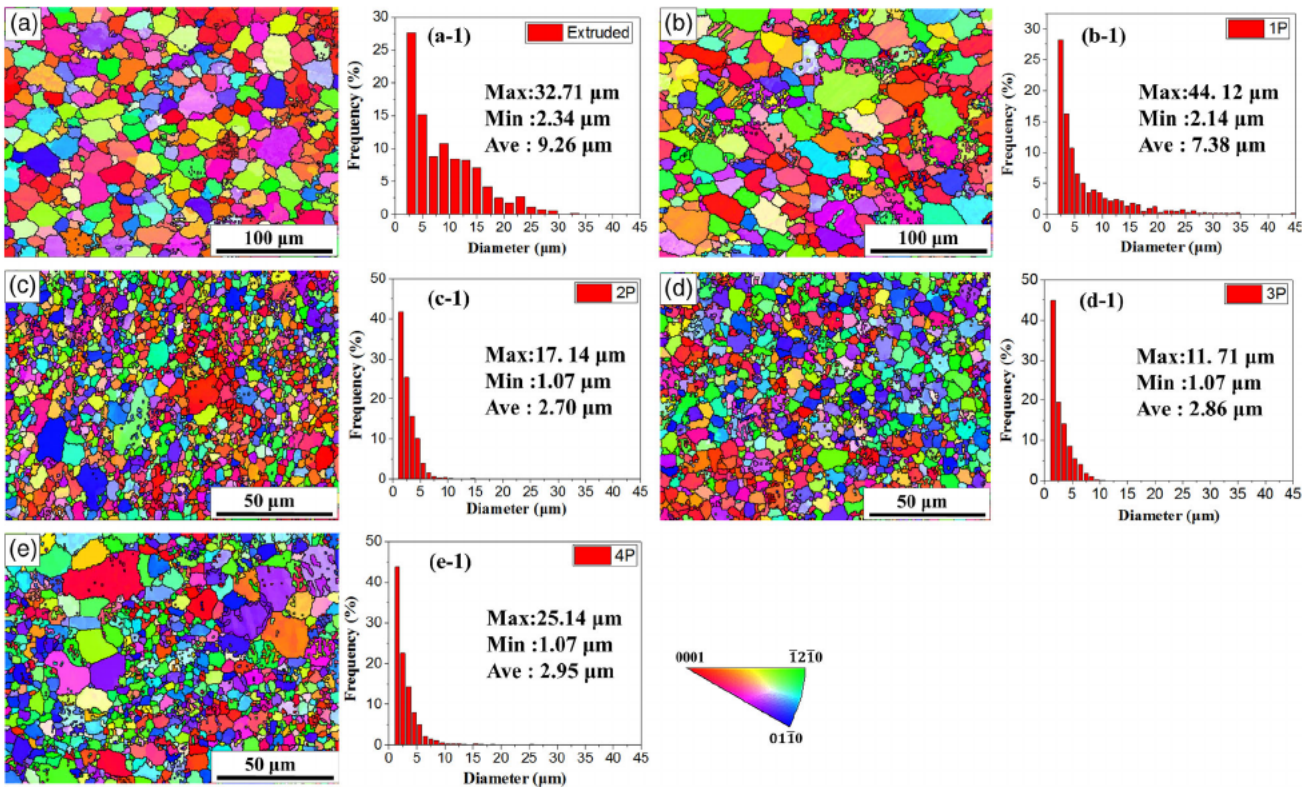

Figure 1. EBSD IPF maps of a) extruded, b) 1P, c) 2P, d) 3P, e) 4P samples; corresponding grain size distributions are shown in (a-1), (b-1), (c-1), (d-1), and (e-1), respectively.

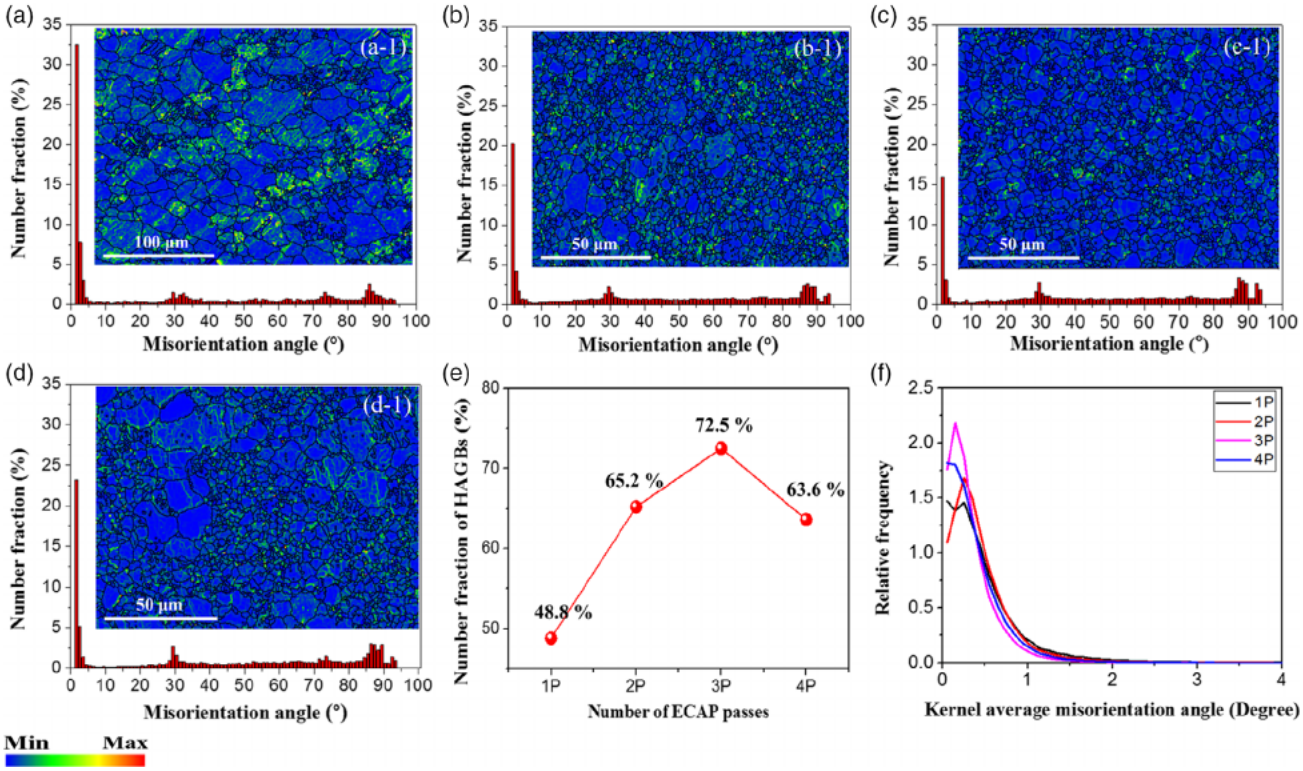

Figure 2. Misorientation angle distribution for a) 1P, b) 2P, c) 3P, and d) 4P samples and KAM maps of (a-1) 1P, (b-1) 2P, (c-1) 3P, and (d-1) 4P samples; f) their corresponding relative frequency. e) Relationship between HAGB ($\theta \geq 15°$) fraction and the number of ECAP passes.

was ≈2.86 μm. When the number of passes increased to four, some grains coarsened obviously.

Figure 2a–d and a-1–d-1 show the distribution of the misorientation angle and kernel average misorientation (KAM) map for the ECAP-processed samples, respectively. The KAM map can estimate the level of residual strain in deformed samples. A rainbow color code in the lower left corner ranges from blue to red denoting minimum to maximum KAM values. As the number of ECAP passes increased from one to three, the area of residual strain concentration gradually diminished and the distribution became more uniform, which can be observed in Figure 2a-1–c-1. Correspondingly, the proportion of high-angle grain boundaries (HAGBs, $\theta \geq 15°$) gradually increased from 48.8% to 72.5%, as shown in Figure 2e. This indicated that the dynamic recrystallization (DRX) became sufficient, which was consistent with the trend of increasingly finer grains from the 1P sample to the 3P sample (Figure 1). However, further increasing the number of ECAP passes to four brought about a decrease of the HAGB proportion and an increase of residual strain, which was mainly because some DRX grains grew after the alloy was subjected to the fourth ECAP pass. The findings of this study are in line with a previously published study by Pan et al.[14] They processed a AZ31B sheet by on-line heating rolling in five passes and found that the grain size reduced and the proportion of HAGBs increased from 67% to 80% in the first three roll passes because of more complete DRX. However, in the last two passes, the grains became coarser, the proportion of HAGBs decreased to 70%, and the deformed grains increased due to the growth of some DRX grains. In addition, Figure 2f reveals that the highest peak of the curve corresponded to a low misorientation angle for the 3P sample, indicating the average KAM value was low and the residual strain was also small.[15] It also confirmed that the most well-developed DRX was obtained in the 3P sample.

Figure 3a–h shows scanning electron microscope (SEM) micrographs of the as-received AZ80M alloy subjected to different ECAP passes. As the number of ECAP passes increased, the second phase became denser. Based on our previous works on the AZ80M alloy[16,17] and related literature,[18] we found that the microstructure of the AZ80M alloy was mainly composed of α-Mg grains and precipitated β-$Mg_{17}Al_{12}$ phases.

2.2. Semisolid Microstructures of ECAP-Processed AZ80M Alloys

As shown in **Figure 4**a–c, in the early stage of semisolid heating (580 °C for 2 min), increasing the number of ECAP passes from one to three could significantly improve the liquid film (liquid phase between solid grains) fraction. Further observation of the microstructure (Figure 4a-1–c-1) reveals that increasing the number of ECAP passes contributed to the penetration of the liquid and the separation of solid grains. However, when further increasing the number of ECAP passes from three to four, there was no obvious difference of the semisolid microstructures between the 4P sample (Figure 4d,d-1) and the 3P sample (Figure 4c,c-1). These phenomena should be related

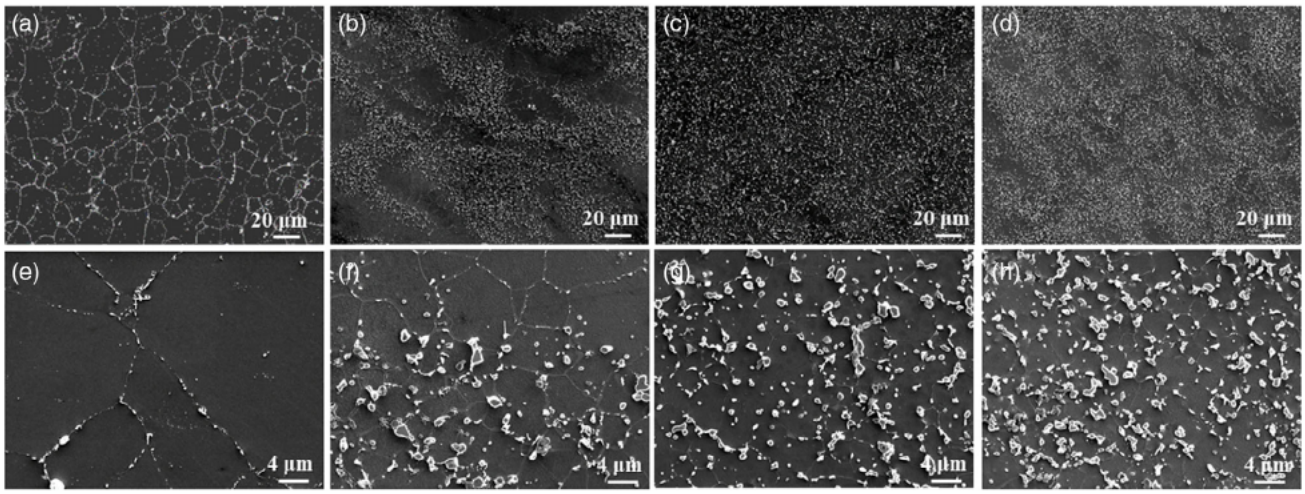

Figure 3. SEM micrographs of a,e) 1P sample, b,f) 2P sample, c,g) 3P sample, d,h) 4P sample.

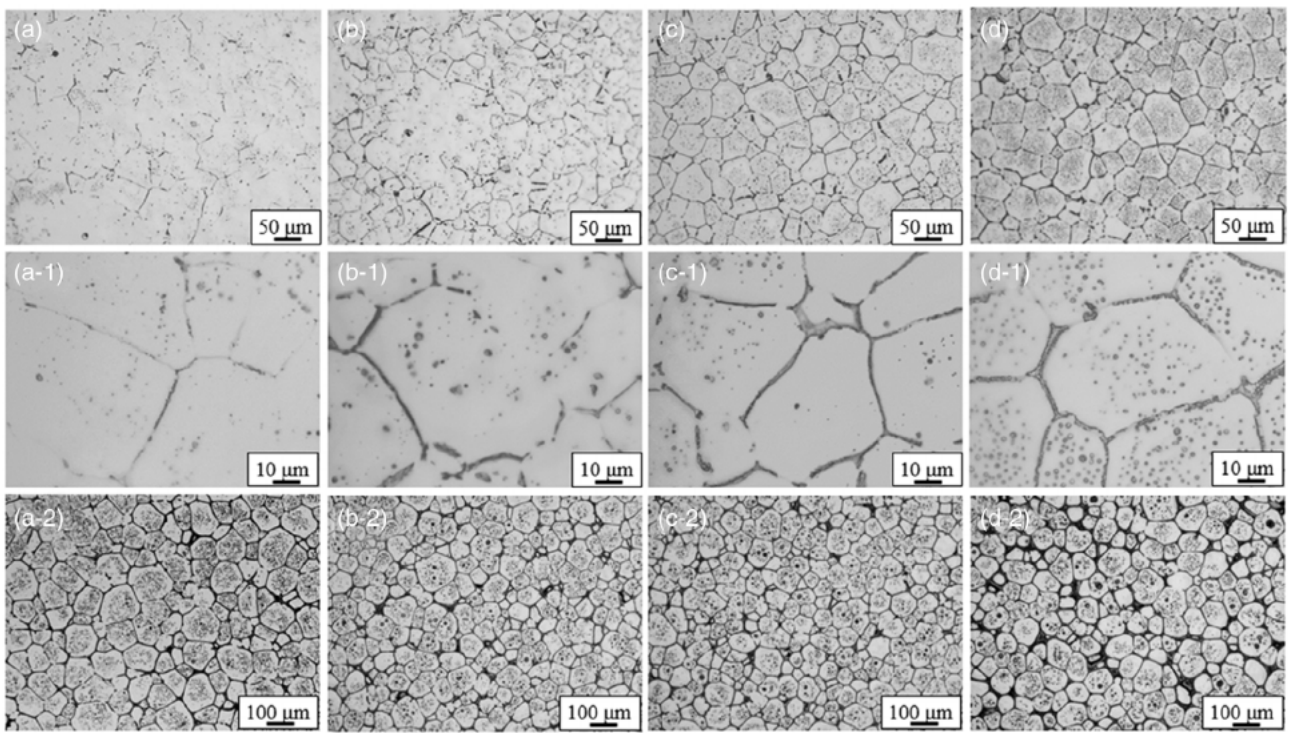

Figure 4. Optical micrographs of a) 1P, b) 2P, c) 3P, and d) 4P samples after isothermal heating at 580 °C for 2 min; (a-1), (b-1), (c-1), and (d-1) are high magnification micrographs of (a), (b), (c), and (d), respectively; Optical micrographs of (a-2) 1P, (b-2) 2P, (c-2) 3P, and (d-2) 4P samples after isothermal heating at 580 °C for 10 min.

to the proportion of HAGBs and the content of the precipitated β-$Mg_{17}Al_{12}$ phase.

According to the Mg–Al binary phase diagrams, the solid solubility of Al in α-Mg increased with the increasing temperature during the heating-up stage below the solidus temperature. Therefore, β-$Mg_{17}Al_{12}$ phases partially dissolved into α-Mg grain under the action of thermal activation. When the temperature rose above the eutectic temperature (437 °C[19]), the residual β-$Mg_{17}Al_{12}$ phases melted.[9,20] If precipitated phases are continuously distributed along the grain boundaries when the temperature rises to the semisolid temperature range, precipitated phases will melt and the liquid phases are connected to each other. As a result, continuous liquid films are formed and the separation of solid grains is achieved. However, it can be observed from Figure 3 that these β-$Mg_{17}Al_{12}$ phases were not continuously distributed along the grain boundaries in the ECAP-processed AZ80M alloy. In this case, whether the liquid formed by the melting of adjacent precipitated phases could

be connected depending on the interfacial energy. When the equation of $2\gamma_{SL} \leq \gamma_{SS}$ is satisfied, the grain boundary (GB) can be penetrated by the liquid phase.[21] In general, HAGBs have higher GB energy than low-angle grain boundaries (LAGBs, $2° \leq \theta < 15°$), so they are more easily infiltrated by the liquid phase. Haghdadi et al.[21] reported that the solid–solid low-energy GBs could not be completely penetrated by the liquid, but HAGBs could be completely wetted. Moradi et al.[22] studied microstructure evolution behavior of ECAP-processed A356 alloy at semisolid reheating temperature and found that the onset of liquid formation occurred at HAGBs. Similarly, Atkinson et al.[23] suggested that during semisolid isothermal heating, DRX occurred first and then the liquid penetrated the DRX boundaries (which were HAGBs), which caused solid grains surrounded by the liquid. However, for the adjacent solid grains with LAGBs, they could not be separated by the liquid and tended to grow by coalescence mechanism.[24] Therefore, after heating the 1–3P samples at 580 °C for 2 min, the infiltration degree of solid grains increased continuously with the increase of ECAP passes, which was primarily attributed to the increase in the proportion of HAGBs from 48.8% to 72.5% and the content of precipitated β-$Mg_{17}Al_{12}$ phases. Although the proportion of HAGBs in the 4P sample (63.6%) was close to that of the 2P sample (65.2%), the semisolid microstructure of the 4P sample exhibited a higher degree of infiltration than the 2P sample, as observed by comparing Figure 4b-1 and d-1. This was mainly caused by more precipitated phases in the 4P sample. Therefore, increase of the HAGB fraction and precipitated β-$Mg_{17}Al_{12}$ phases in the initial microstructure was favorable for the liquid phase to penetrate more grain boundaries in the early stage of semisolid heating.

When the 1P sample was isothermally heated at 580 °C for 10 min (Figure 4a-2), a substantial amount of coarse and irregular solid grains could be seen in the sample. This is mainly because the adjacent solid grains with a low misorientation angle tend to grow by coalescence mechanism at a high solid fraction, leading to the formation of coarse solid grains with an irregular shape. Only a few coarse solid grains existed in the 2P sample after isothermal heating at 580 °C for 10 min and the shape of most of the solid grains became more equiaxed (Figure 4b-2). However, coarse and irregular solid grains could hardly be found in the 3P sample after isothermal heating at 580 °C for 10 min (Figure 4c-2). It demonstrated that a larger proportion of HAGBs and higher precipitated phase content in the deformed sample could effectively prevent the coalescence of adjacent solid grains, which could retard the coarsening process at a high solid fraction. For the 4P sample after isothermal heating at 580 °C for 10 min (Figure 4d-2), the size of solid grains increased slightly and the volume fraction of the liquid phase increased perceptibly. Comparing Figure 4a-2–d-2, it can be found that the liquid mainly existed near smaller solid grains, and the liquid fraction in Figure 4a-2–c-2 was significantly less than in Figure 4d-2. The phenomenon can be explained by the coarsening mechanism. When the 3P and 4P samples were heated at 580 °C for 2 min, continuous liquid films formed around the solid grains, and liquid diffusion channels were established. As the isothermal time was extended to 10 min, liquid diffusion was promoted. In this case, the Ostwald ripening mechanism began to work. Ostwald ripening is a coarsening process in which large grains grow by consuming small grains when the size of two globular grains differs greatly.[25] In the process of Ostwald ripening, small solid grains gradually melt, which promotes the formation of more liquid.[25] Therefore, the higher the nonuniformity of the grain size was in the deformed sample, the more conducive the Ostwald ripening process would be during the subsequent semisolid heating, resulting in the formation of more liquid phase. Therefore, the 3P sample with excellent grain-size uniformity shown in Figure 1d,d-1 had a lower liquid fraction than the 4P sample with poor grain-size uniformity shown in Figure 1e,e-1. However, when the 1P and 2P samples were heated at 580 °C for 2 min, liquid films were discontinued and solid grains were interconnected. As the isothermal temperature was prolonged, the primary coarsening mechanism was the coalescence mechanism, which resulted in the scanty liquid phase.

Figure 5 shows the result of quantifying the effects of the number of ECAP passes on semisolid microstructure characteristics (average grain size (Deq) and shape factor (SF)) of the AZ80M alloy in the subsequent stages of semisolid heating (580 °C for 10–35 min). Under different soaking times, the effect of the number of ECAP passes on Deq and SF showed a similar trend. Increasing the number of ECAP passes from one to three

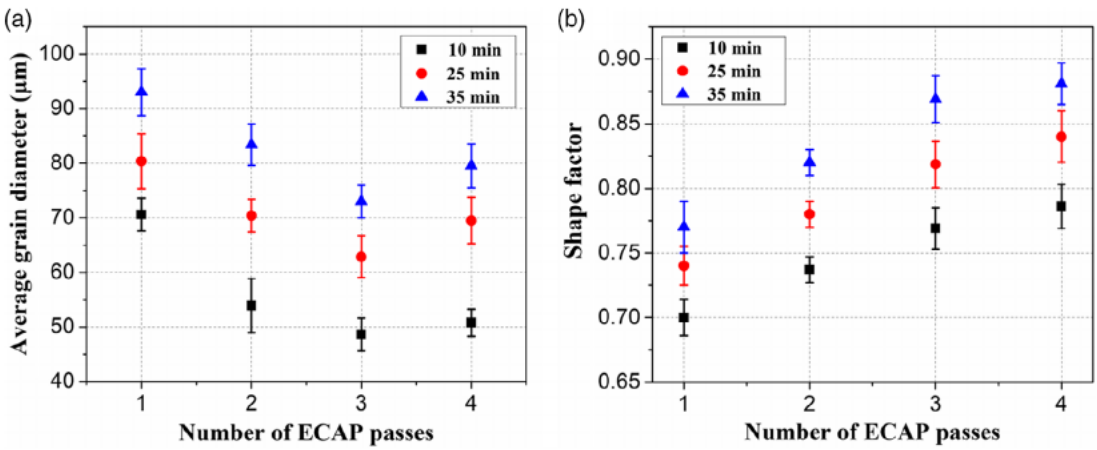

Figure 5. Variation of a) average grain size and b) SF versus the number of ECAP passes for samples subjected to ECAP and then heated at 580 °C for various soaking times.

led to an apparent downward trend for the Deq value and upward trend for the SF value. However, with a further increase in the number of ECAP passes to four, the upward trend of the SF value became gentler, and a slight increase occurred in the Deq value. Thus, when the alloy was subjected to four passes of ECAP, the solid grains were not further refined and the roundness of the solid grains was improved marginally.

2.3. Coarsening Kinetics of ECAP-Processed AZ80M Alloys with Different Passes

Generally, the Lifshize–Slorovitze–Wagner (LSW) theory has been applied to study the coarsening behavior of solid grains in a semisolid system.[26] According to the LSW theory, the growth kinetics of solid grains can be described as follows

$$D_t^n - D_0^n = Kt \tag{1}$$

where D_t^n is the average grain size after soaking time t, D_0^n is the initial grain size before semisolid isothermal heating, K is the coarsening rate coefficient, and n is the diffusion exponent. According to previous research,[11–13] the value of n was selected as 3 for the grain coarsening behavior of a semisolid metal.

Figure 6a–d shows the cube of the Deq value as a function of the soaking time for the ECAP-processed samples treated at 560, 580, and 600 °C. The K values and regression coefficient (R^2) obtained from fitting results of Figure 6a–d are given in

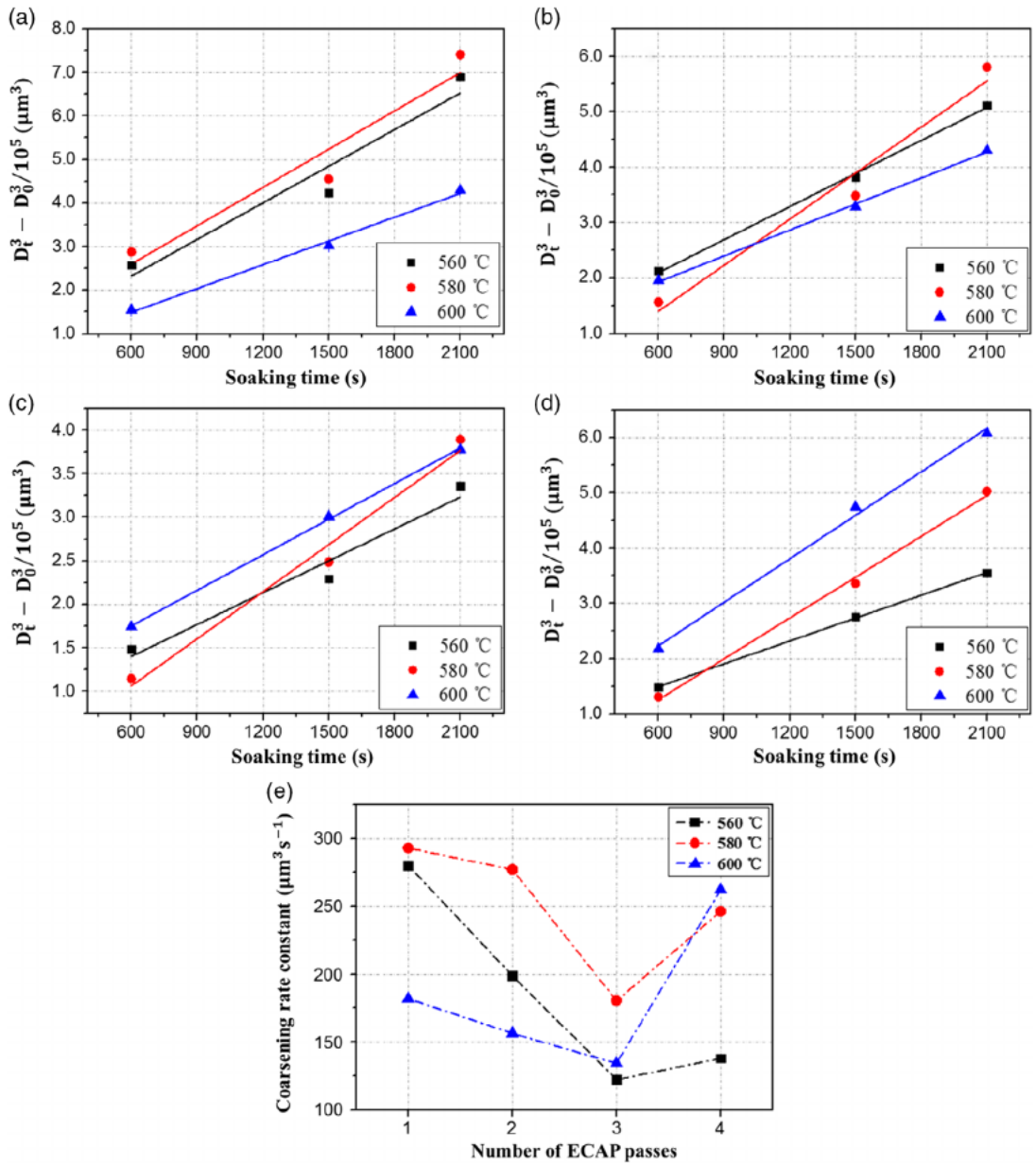

Figure 6. Cube of average grain size as a function of soaking time for a)1P, b) 2P, c) 3P, and d) 4P samples treated at 560, 580, and 600 °C; e) the variation of coarsening rate constants (K) of ECAP-processed samples with the number of ECAP passes at 560, 580, and 600 °C.

Table 1. Coarsening rate constant (K) and regression coefficient (R^2) values at different isothermal temperatures for AZ80M alloy processed using one to four passes of ECAP.

Temperature [°C]	One pass		Two passes		Three passes		Four passes	
	K [$\mu m^3\ s^{-1}$]	R^2	K [$\mu m^3\ s^{-1}$]	R^2	K [$\mu m^3\ s^{-1}$]	R^2	K [$\mu m^3\ s^{-1}$]	R^2
560	279.9	0.877	198.7	0.997	121.9	0.925	137.8	0.999
580	292.7	0.864	276.9	0.944	180.3	0.967	246.2	0.994
600	181.7	0.988	156.1	0.997	134.1	0.999	262.1	0.991

Table 1. Figure 6e shows the variation of the K values of ECAP-processed samples with the number of ECAP passes at different isothermal temperatures (560, 580, and 600 °C). As the number of ECAP passes increased at different holding temperatures, the K values of ECAP-processed samples showed a similar trend of going downward and then upward. The trend in this study was different from the previous results based on RUE-processed 7075Al,[11] ECAP-processed 7075Al,[12] and compression specimens of 7075Al.[13]

Generally, the coarsening of solid grains in semisolid alloys is considered to be controlled by grain coalescence and Ostwald ripening mechanisms.[27] When the solid fraction is high, the role of diffusion is limited because of the scant liquid phase. Coarsening proceeds first through the coalescence of adjacent solid grains with perfectly matched crystallographic orientations. In this study, as shown in **Figure 7**a–h, the solid-grain coarsening of ECAP-processed AZ80M alloys with different passes was mainly controlled by the solid–solid contacts rather than by diffusion through the liquid at a high solid fraction (560 °C, $f_S = 0.72$). Therefore, at the isothermal temperature of 560 °C, the coarsening process of the ECAP-processed AZ80M alloy was primarily controlled by coalescence mechanism. Figure 6e shows that at 560 °C, the coarsening rate of the AZ80M alloy decreased significantly as the ECAP passes increased from one to three. It should be attributed to the obvious increase of HAGB proportion in the initial microstructure, which hindered the coalescence of the adjacent solid grains. However, as the

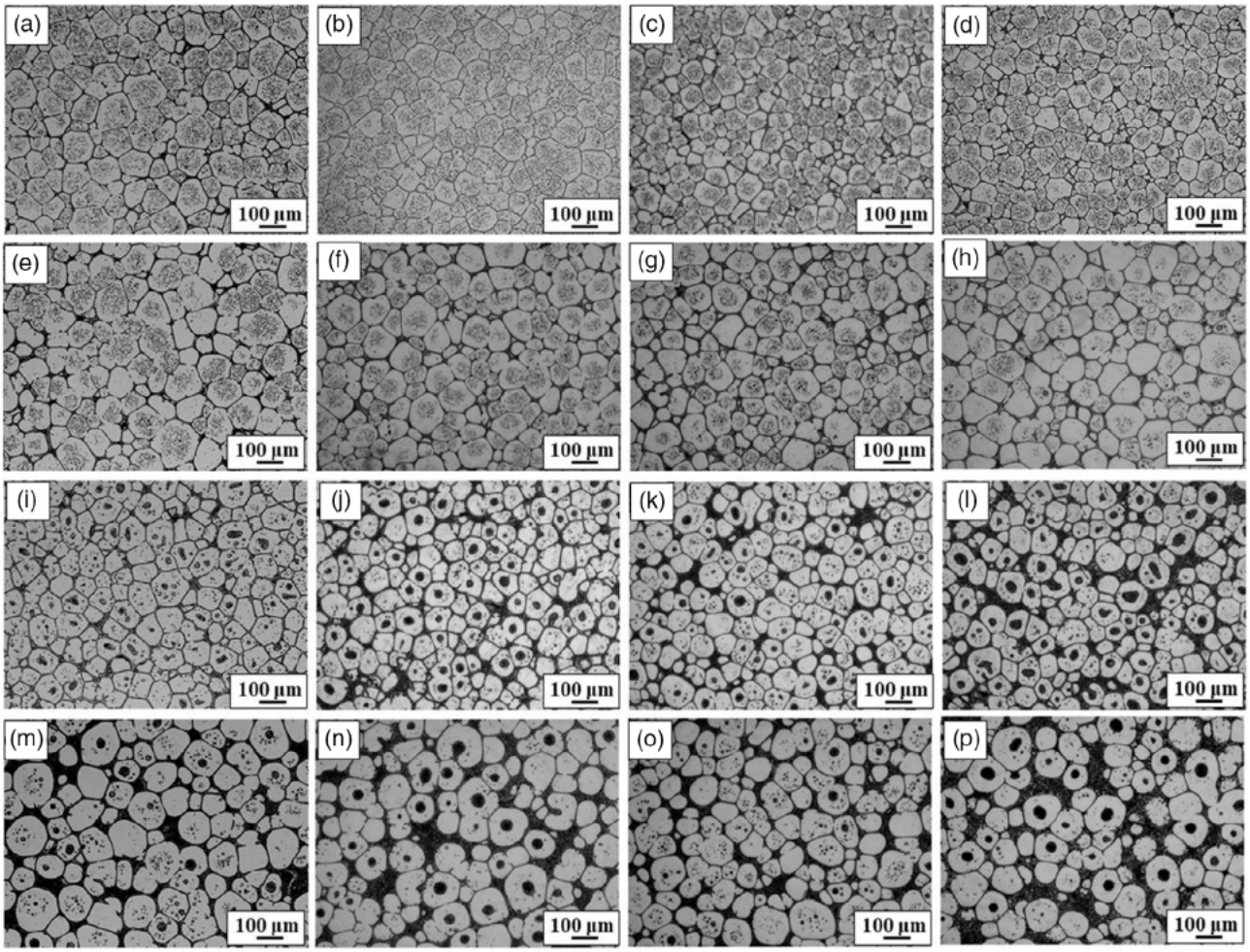

Figure 7. Semisolid microstructure of a) 1P, b) 2P, c) 3P, and d) 4P samples after isothermal heating at 560 °C for 10 min. Semisolid microstructure of e) 1P, f) 2P, g) 3P, and h) 4P samples after isothermal heating at 560 °C for 25 min. Semisolid microstructure of i) 1P, j) 2P, k) 3P, and l) 4P samples after isothermal heating at 600 °C for 10 min. Semisolid microstructure of m) 1P, n) 2P, o) 3P, and p) 4P samples after isothermal heating at 600 °C for 25 min.

ECAP passes further increased to four, the coarsening rate of the AZ80M alloy increased. This was consistent with the decrease in HAGB proportion in the 4P sample, although we discussed in Section 2.2 and concluded that the content of the precipitated phase and the proportion of HAGBs would affect the degree of solid grains being infiltrated and separated, thereby hindering the process of coalescence coarsening. However, the K value of the 4P sample was higher than that of the 3P sample, indicating that the influence of the HAGB proportion on the coalescence coarsening process was more dominant.

With the increase of the isothermal temperature (580 °C), the downward trend of the K values from the 1P to 3P samples progressively decreased. This could be explained by the fact that the formation of more liquid would lower solid–solid contacts and weaken the coalescence mechanism of solid grains at higher temperatures. The phenomenon has been confirmed in previous studies.[12,13] Therefore, the hindering effect of HAGBs on coalescence coarsening at a higher temperature (580 °C) was not as apparent as that at a low temperature (560 °C). However, as the ECAP passes increased further from three to four, the coarsening rate of the AZ80M alloy increased. This may be caused by the transformation of the coarsening mechanism to Ostwald ripening in the semisolid 4P sample. Based on previous research on recrystallization and partial melting (RAP) 7075Al[12] and SIMA 7075Al,[13] it was found that the K value first decreased and then increased as the result of the coarsening mechanism transition from coalescence to Ostwald ripening.

As the isothermal heating temperature increased further to 600 °C and the liquid fraction increased significantly, the coarsening process of solid grains was controlled by liquid diffusion. On the one hand, the elevating of the isothermal temperature provided more energy for diffusion, and on the other hand, liquid provided a much faster diffusion path than solid. In this case, Ostwald ripening played a leading role in solid-grain coarsening. It can be seen from Figure 7i–p that the solid-grain coarsening of ECAP-processed AZ80M alloys with different passes was mainly controlled by diffusion through the liquid at a low solid fraction (600 °C, $f_S = 0.29$). The Ostwald ripening is controlled by the Gibbs–Thompson effect, which changes the concentration of the solid–liquid interface according to the curvature of the interface, thereby creating a concentration gradient and leading to the diffusion transport of the material.[25] Therefore, the concentration degree of Al solute in the liquid around small solid grains was below that around large solid grain, which means that the concentration gradient existed between small and large solid grains. Therefore, the larger the difference in the size of the adjacent solid grains was, the higher was the proportion of small grains and the greater was the curvature difference of the adjacent solid grains. It contributed to the greater concentration gradient of the solute in the liquid phase around the adjacent solid grains, which provided a higher driving force for Ostwald ripening, resulting in a faster coarsening rate. Figure 6e shows that at 600 °C, the coarsening rate of the AZ80M alloy decreased gradually as the ECAP passes increased from one to three, which could be ascribed to the increasing uniformity of the initial grain size. As the ECAP passes further increased to four, the coarsening rate of the AZ80M alloy increased sharply. The obvious coarsening in the 4P sample was mainly because of the obvious coarsening of some DRX grains, but there were still many fine DRX grains, resulting in a large difference in grain size.

2.4. Comparison of Coarsening Kinetics of Semisolid Mg Alloys Prepared by Different Routes

Figure 8 summarizes the coarsening kinetics of semisolid Mg alloys processed by different routes.[9,27–35] It can be found that the K values of the semisolid alloys were significantly affected by the different routes. The K values of the same series of Mg alloys prepared by different processes were compared as follows.

For AZ91 alloys, $K_{(RUE)} > K_{(ECAP\text{-}2P)} > K_{(MAF)} > K_{(ECAP\text{-}4P)}$, the K values of each route were as follows: $K_{(RUE)} = (314\ \mu m^3\ s^{-1}$ at $f_S = 0.7)$;[9] $K_{(ECAP\text{-}2P)} = (268\ \mu m^3\ s^{-1}$ at $f_S = 0.7)$;[29] $K_{(MAF)} = (202\ \mu m^3\ s^{-1}$ at $f_S = 0.7)$;[28] and $K_{(ECAP\text{-}4P)} = (167\ \mu m^3\ s^{-1}$ at $f_S = 0.55)$;[30]

For AZ80 alloys, $K_{(RUE)} > K_{(ECAP\text{-}3P)}$, the K values of each route were as follows: $K_{(RUE)} = (248\ \mu m^3\ s^{-1}$ at $f_S = 0.78)$[31] and $K_{(ECAP\text{-}3P)} = (122\ \mu m^3\ s^{-1}$ at $f_S = 0.72)$.

For AM60 alloys, $K_{(MAF)} > K_{(ECAP\text{-}4P)}$, the K values of each route were as follows: $K_{(MAF)} = (309\ \mu m^3\ s^{-1}$ at $f_S = 0.65)$[32] and $K_{(ECAP\text{-}4P)} = (52\ \mu m^3\ s^{-1}$ at $f_S = 0.8)$.[33]

For ZK60 alloys, $K_{(RAP)} > K_{(ECAP\text{-}4P)}$, the K values of each route were as follows: $K_{(RAP)} = (556\ \mu m^3\ s^{-1}$ at $f_S = 0.7)$;[34] $K_{(RAP)} = (317\ \mu m^3\ s^{-1}$ at $f_S = 0.8)$;[35] $K_{(ECAP\text{-}4P)} = (255\ \mu m^3\ s^{-1}$ at $f_S = 0.75$; $371\ \mu m^3\ s^{-1}$ at $f_S = 0.65)$.[27]

Based on the aforementioned comparison results, it can be concluded that ECAP-processed Mg alloys generally had lower K values compared to materials processed by other routes. The possible reasons were analyzed and might be as follows.1) A high proportion of HAGBs in the deformed sample hindered the coalescence of the adjacent solid grains at high solid fractions, which led to a low coarsening rate. The RUE and multi-axial forging (MAF) processes decrease the size of the initial ingots during deformation, so the strain introduced into the blank is limited. However, ECAP is a severe plastic deformation (SPD) method, which can introduce higher strain without shape and dimension variations. According to previous research,[36]

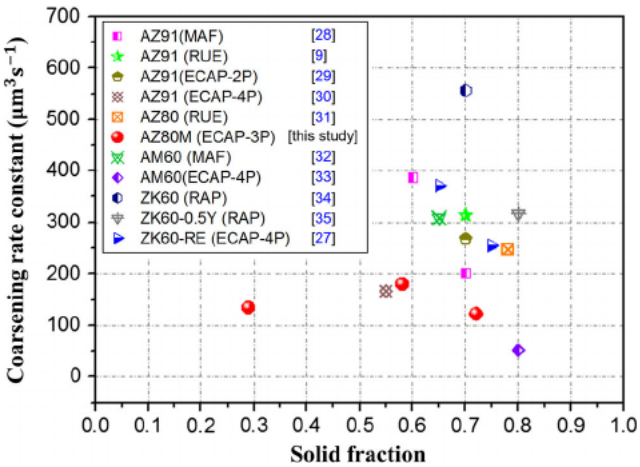

Figure 8. Comparison of coarsening rate constants (K) versus solid fractions (f_S) for Mg alloys subjected to different routes.

higher strain provides a higher driving force for recovery and recrystallization, thereby forming larger area recrystallization nucleation. And recrystallization nucleation means the formation and migration of HAGBs. Generally, alloys subjected to ECAP usually have a relatively high proportion of HAGBs.[37] Therefore, the ECAP-processed Mg alloys had a lower coarsening rate than those treated by RUE and MAF, which is attributed to a relatively high proportion of HAGBs in ECAP-processed samples. Similarly, Wang et al.[38] compared the K values of 7075Al alloys processed using friction stir processing (FSP), SIMA, and RAP. They found that the K value of the FSP-processed alloy was much lower than that of SIMA- and RAP-processed alloys, which was mainly because of the larger proportion of HAGBs caused by the FSP process. 2) Uniform and fine grains in the deformed sample resulted in an insufficient driving force for the Ostwald ripening process at low solid fractions, which also led to a low coarsening rate. Therefore, the introduction of those SPDs can significantly improve not only the HAGB proportion in the initial microstructure of the alloy, but also refined and homogenized grains. These can effectively lower the coarsening rate of semisolid alloys and assist in the preparation of a semisolid slurry. ECAP was demonstrated to be an efficient method at facilitating semisolid Mg alloy billets with a low coarsening rate.

3. Conclusions

In this study, semisolid samples of the AZ80M magnesium alloy were fabricated using ECAP followed by semisolid isothermal heating treatment. The effect of the number of ECAP passes on the coarsening kinetics of the AZ80M alloy at different semisolid heating temperatures was systematically investigated. The K values of the semisolid Mg alloys produced using different routes were compared and discussed. The main conclusions are summarized subsequently. 1) The increase in the number of ECAP passes from one to three resulted in a significant reduction in grain size and an increase in the proportion of HAGBs due to increasingly full DRX. In contrast, up to four passes caused an increase in grain size and a decrease in the proportion of HAGBs due to the growth of some DRX grains. 2) As the number of ECAP passes increased at different holding temperatures, the K values of ECAP-processed samples showed a similar trend of going downward and then upward. And the K value of the sample after three passes of ECAP processing (3P) was the lowest. It was primarily attributed to the maximum HAGB proportion and the most uniform grain size in the deformed samples. At high solid fractions, a high proportion of HAGBs in the deformed sample hindered the coalescence of the adjacent solid grains, which led to a low coarsening rate. At low solid fractions, uniform and fine grains in the deformed sample resulted in an insufficient driving force for the Ostwald ripening process, which led to a low K value. 3) ECAP was demonstrated to be an efficient method at facilitating semisolid Mg alloy billets with a low coarsening rate. It could improve the fraction of HAGBs and obtain fine and homogeneous grains in the initial microstructure, thereby retarding the grain coarsening of semisolid alloys.

4. Experimental Section

Starting Materials and Calculation of the Solid Fraction: The starting materials used in this work were extruded rods (Φ30 mm) of AZ80–0.2Y–0.15Ca wt% (AZ80M) magnesium alloy. The semisolid temperatures of AZ80M alloy were selected as 560, 580, and 600 °C. The specific composition of the starting material and the reason for the selection of the semisolid temperature are described in a previous study.[16] The theoretical liquid fraction (f_L) values corresponding to different semisolid temperatures can be calculated using the Scheil equation[39]

$$f_L = \left(\frac{T_M - T_L}{T_M - T}\right)^{1/(1-k)} \tag{2}$$

where T_M is the melting point of pure magnesium (650 °C),[40] T_L is the liquidus temperature of the AZ80M alloy (610 °C),[16] T is the isothermal heating temperature, and k is the equilibrium distribution coefficient. The k value can be calculated by the following equation[40]

$$k = \frac{\sum m_i c_i k_i}{\sum m_i c_i} \tag{3}$$

where c_i represents the content of element (i) in the alloy composition, m_i represents the liquidus slope of the Mg–i binary alloy, and k_i represents the diffusion coefficient of element (i) in Mg. In the AZ80M alloy composition, $m_{Al} = -6.87$, $m_{Zn} = -0.64$, $m_Y = -3.4$, $m_{Ca} = -12.67$, $k_{Al} = 0.37$, $k_{Zn} = 0.12$, $k_Y = 0.50$, and $k_{Ca} = 0.06$.[40] Therefore, the calculated k value of the AZ80M alloy was 0.356. So the liquid fractions corresponding to the semisolid temperatures of 560, 580, and 600 °C were 0.28, 0.42, and 0.71, respectively.

ECAP Deformation: Cuboid 20 mm × 20 mm × 70 mm samples were machined from the center of the as-extruded materials and prepared for ECAP. In this work, the AZ80M samples were subjected to one pass, two passes, three passes, or four passes of ECAP using route Bc (the sample was rotated by 90° in the clockwise direction between passes), which were labeled as "1P," "2P," "3P," and "4P" samples, respectively. The ECAP die was fabricated from H13 steel with an internal angle (φ) of 90° and external angular (Ψ) of 37°. Before ECAP, the cuboid specimens were preheated at 320 °C for 15 min. A heating jacket was placed around the die to control the extrusion temperature to a set value of 320 ± 5 °C. A thermometer was used to monitor the temperature. Both the die and specimens were lubricated with molybdenum disulfide (MoS_2) to reduce friction. After each extrusion pass, the deformed samples treated by ECAP were immediately quenched in cold water.

Isothermal Treatment Test and Microstructure Characterization: For the isothermal treatment, semisolid samples with a radius of 8 mm and a height of 12 mm were machined from the ECAP deformed billets parallel to the extrusion direction. The samples were isothermally heated at various semisolid temperatures of 560, 580, and 600 °C for 2–35 min. The quantitative analysis method of semisolid microstructure (the SF and Deq) have also been described in detail in a previous article.[16] The observation surface of all microstructures was perpendicular to the extrusion direction in this study.

The samples were polished and etched with a picric acid solution (2.75 g picric acid, 2.5 mL acetic acid, 45 mL ethyl alcohol, and 5 mL distilled water). The microstructure of the samples prepared by ECAP and then semisolid isothermal treatment was observed using an optical microscope (OM, ZEISS Axio Lab. A1) and a field emission scanning electron microscope (FESEM, JEOL JSM 7800F). The observed second-phase particles were identified by an X-Max 80 energy dispersive X-ray spectrometer (EDS, Oxford). EBSD was conducted to measure the initial microstructure of deformed samples using an SEM equipped with an Oxford Instrument Nordlys Nano EBSD detector and HKL channel 5 data acquisition software.

Acknowledgements

This work was supported by the China Scholarship Council (201807000021), Key Development Project of Sichuan Province (grant number 2017GZ0399), the 2017 Doctoral Innovation Fund Program of Southwest Jiaotong University (grant number D-CX201733), and the Innovative & Practice Project of Graduate School of Southwest Jiaotong University (grant number 2018KXK05). The authors acknowledge the equipment support from Litmat Technology Chengdu Co., Ltd.

Conflict of Interest

The authors declare no conflict of interest.

Keywords

AZ80M, coarsening kinetics, coarsening mechanism, equal channel angular pressing, high-angle grain boundaries

Received: April 6, 2020
Revised: July 20, 2020
Published online:

[1] M. K. Kulekci, *Int. J. Adv. Manuf. Technol.* **2008**, *39*, 851.
[2] S. Fida Hassan, M. T. Islam, S. Nouari, N. Al-Aqeeli, M. M. A. Baig, F. Patel, *J. Alloys Compd.* **2019**, *787*, 1015.
[3] L. B. Ren, J. Wu, G. F. Quan, *Mater. Sci. Eng. A* **2014**, *612*, 278.
[4] S. M. Mirghasemi, A. R. Eivani, S. H. Seyedein, H. R. Jafarian, *Eng. Fract. Mech.* **2018**, *199*, 721.
[5] S. Chayong, H. V. Atkinson, P. Kapranos, *Mater. Sci. Eng. A* **2005**, *390*, 3.
[6] Y. Xu, C. Chen, J. B. Jia, X. X. Zhang, H. H. Dai, Y. Yang, *J. Alloys Compd.* **2018**, *748*, 694.
[7] L. P. Wang, T. Chen, W. Y. Jiang, Y. C. Feng, W. X. Dong, Z. W. Wang, Z. Q. Liang, Y. Zhu, *J. Rare Earths* **2013**, *31*, 319.
[8] C. T. W. Proni, L. V. Torres, R. Haghayeghi, E. J. Zoqui, *Mater. Charact.* **2016**, *118*, 252.
[9] Y. Xu, L. X. Hu, J. B. Jia, B. Xu, *Mater. Charact.* **2016**, *118*, 309.
[10] J. L. Fu, H. J. Jiang, K. K. Wang, *Acta Metall. Sin.* **2018**, *31*, 337.
[11] B. Binesh, M. Aghaie-Khafri, *Mater. Des.* **2016**, *95*, 268.
[12] J. L. Fu, S. X. Wang, K. K. Wang, *J. Mater. Sci.* **2018**, *53*, 9790.
[13] B. Binesh, M. Aghaie-Khafri, *Mater. Charact.* **2015**, *106*, 390.
[14] F. S. Pan, B. Zeng, B. Jiang, A. Atrens, H. W. Dong, *Mater. Charact.* **2017**, *124*, 266.
[15] Z. Q. Yang, A. B. Ma, H. Liu, D. Song, Y. N. Wu, Y. C. Yuan, J. H. Jiang, J. P. Sun, *Mater. Charact.* **2019**, *152*, 213.
[16] L. L. Fan, M. Y. Zhou, Y. W. X. Zhang, Q. Tang, G. F. Quan, B. Liu, *Mater. Charact.* **2019**, *154*, 116.
[17] L. B. Ren, G. F. Quan, M. Y. Zhou, Y. Y. Guo, Z. Z. Jiang, Q. Tang, *Mater. Sci. Eng. A* **2017**, *690*, 195.
[18] D. G. Zhao, Z. Q. Wang, M. Zuo, H. R. Geng, *Mater. Des.* **2014**, *56*, 589.
[19] M. Fatmi, A. Djemli, A. Ouali, T. Chihi, M. A. Ghebouli, H. Belhouchet, *Results Phys.* **2018**, *10*, 693.
[20] S. Kleiner, O. Beffort, P. J. Uggowitzer, *Scr. Mater.* **2004**, *51*, 405.
[21] N. Haghdadi, A. Zarei-Hanzaki, S. Heshmati-Manesh, H. R. Abedi, S. B. Hassas-Irani, *Mater. Des.* **2013**, *49*, 878.
[22] M. Moradi, M. Nili-Ahmadabadi, B. Poorganji, B. Heidarian, M. H. Parsa, T. Furuhara, *Mater. Sci. Eng. A* **2010**, *527*, 4113.
[23] H. V. Atkinson, K. Burke, G. Vaneetveld, *Mater. Sci. Eng. A* **2008**, *490*, 266.
[24] E. Rabkin, I. Snapiro, *Acta Mater.* **2000**, *48*, 4463.
[25] J. G. Wang, H. Q. Lin, H. Y. Wang, Q. C. Jiang, *J. Alloys Compd.* **2008**, *466*, 98.
[26] I. M. Lifshitz, V. V. Slyozov, *J. Phys. Chem. Solids* **1961**, *19*, 35.
[27] Z. D. Zhao, Q. Chen, Y. B. Wang, D. Y. Shu, *Mater. Sci. Eng. A* **2009**, *506*, 8.
[28] H. Q. Ning, F. F. Peng, S. F. Zhu, Q. H. Hu, Z. R. Li, J. Zhao, Q. Zhao, S. D. Huang, X. Jin, *Mater. Res. Innovations* **2013**, *17*, 16.
[29] Q. Chen, S. J. Luo, Z. D. Zhao, *J. Alloys Compd.* **2009**, *477*, 726.
[30] T. J. Chen, Y. K. Ma, Y. D. Li, G. X. Lu, Y. Z. Hao, *Mater. Sci. Technol.* **2010**, *26*, 1197.
[31] Q. Chen, Z. D. Zhao, Z. X. Zhao, C. K. Hu, D. Y. Shu, *J. Alloys Compd.* **2011**, *509*, 7303.
[32] Q. Chen, Z. D. Zhao, G. Chen, B. Wang, *J. Alloys Compd.* **2015**, *632*, 190.
[33] J. F. Jiang, Y. Wang, J. J. Qu, Z. M. Du, Y. Sun, S. J. Luo, *J. Alloys Compd.* **2010**, *497*, 62.
[34] S. J. Luo, Q. Chen, Z. D. Zhao, *Mater. Sci. Eng. A* **2009**, *501*, 146.
[35] Z. D. Zhao, Q. Chen, H. Y. Chao, S. H. Huang, *Mater. Des.* **2010**, *31*, 1906.
[36] P. R. Rios, F. Siciliano, H. R. Z. Sandim, R. L. Plaut, A. F. Padilha, *Mater. Res.* **2005**, *8*, 225.
[37] M. Suresh, A. Sharma, A. M. More, R. Kalsar, A. Bisht, N. Nayan, S. Suwas, *J. Alloys Compd.* **2019**, *785*, 972.
[38] K. Wang, Z. M. Zhang, H. Wen, D. Xia, W. J. Sun, *Mater. Charact.* **2016**, *121*, 1.
[39] Q. Q. Zhang, Z. Y. Cao, Y. F. Zhang, G. H. Su, Y. B. Liu, *J. Mater. Process Tech.* **2007**, *184*, 195.
[40] Y. C. Lee, A. K. Dahle, D. H. StJohn, *Metall. Mater. Trans. A* **2000**, *31*, 2895.